Journal of Ceramic Processing Research. Vol. 24, No. 6, pp. 947~953 (2023)
(Received 30 July 2023, Received in revised form 11 October 2023, Accepted 15 October 2023)
https://doi.org/10.36410/jcpr.2023.24.6.947

J O U R N A L O F
Ceramic Processing Research

Microstructure and wear behavior of WC-30WB-10Co cemented carbide coating sprayed by HVOF

Baogang Liu[a,*], Sam Lu[b] and Haifan Zhu[a]
[a]*School of Energy and Electromechanical Engineering, Hunan University of Humanities, Science and Technology, No.487, Dixing Road, Loudi, Hunan 417000, China*
[b]*Henan Clark Industrial Co., Ltd, Zhengzhou 45000, China*

Numerous studies have been made to enhance the wear resistance of WC-Co coatings deposited by HVOF during the last few years. Spherical WC-30WB-10Co powders were firstly fabricated by agglomeration and sintering process, which were then employed to deposit coating by HVOF. The morphologies, phase composition, hardness, as well as sliding wear performance of the as-deposited coatings were explored. The same experiments were carried out on traditional WC-12Co coatings with the purpose of making the comparison. The results showed that the CoWB compound was formed through the reaction between Co and WB in the sintering process of the WC-30WB-10Co powders. The diffraction peaks of W_2C, Co_3W_3C and Co_6W_6C were found in the XRD patterns of both coatings, implying that oxidation and decarburization happened in the spraying process of both powders. In relative to the traditional WC-12Co coating, the microhardness and wear resistance of the WC-30WB-10Co coating were greatly enhanced. Obviously, with the microhardness of the WC-30WB-10Co coating being elevated by 34.1%, the wear rates were only 49.3% of that of WC-12Co coatings. This was resulted from the existence of the superhard CoWB phase in the WC-30WB-10Co coating. The wear mechanisms of both coatings were abrasive wear and oxidative wear.

Keywords: Coating, Microstructure, Wear, High velocity oxy-fuel spraying.

Introduction

WC-Co coatings deposited by HVOF is regarded as one of the most widely used coatings for wear protection due to its good mechanical and wear properties [1-3]. The applications of WC-Co coatings have been expanded to different areas such as aerospace, metallurgy, oil drilling, as well as sea engineering [4-7]. Recently, with the purpose of further strengthening the wear resistance of WC-Co coatings deposited by HVOF, many efforts have been undertaken. Wang, et al. prepared spherical and fully densified WC-Co particles with the use of alumina-assisted treatment method, and found that in relative to that of the conventional coating, the wear resistance of the prepared coating using the particles by HVOF was approximately 4 times higher [8]. Mohanty et al. explored the tribological properties of 1 wt% carbon nanotube reinforced HVOF sprayed WC-Co coatings. The obtained findings showed that the wear resistance of the reinforced coatings was notably enhanced in relative to those of the coatings without carbon nanotube [9]. Mi et al. reported the impact of heat treatment on microstructure and wear performance of WC-Co coating sprayed by HVOF, pointing out that the heat-treated coating at 450 °C exhibited lower porosity and better wear resistance than the as-deposited coating [10]. The wear performance of WC-Co coatings exerted a vital function in the practical application [11]. Design of material components played an important role in improving wear resistance of WC-Co coating. Additionally, the microhardness of WB was about 40 GPa, which was over two times higher than WC [12, 13]. In view of this, through the addition of WB into WC-Co powders, the hardness and wear resistance of WC-Co coating can be strengthened.

Therefore, this work was aimed at evaluating the impact of WB addition on microstructure, microhardness and wear resistance of WC-Co coating. Therefore, the spherical WC-30WB-10Co powders were prepared. In the meanwhile, HVOF was used to deposit the corresponding coatings. Using XRD and SEM, the microstructure of the WC-30WB-10Co coating was characterized. In addition, we also explored the mechanical properties and wear behavior of the coating. Apart from that, the same experiments were carried out on traditional WC-12Co coatings for the purpose of comparison.

*Corresponding author:
Tel : (86-738)8326910
Fax: (86-738)8326910
E-mail: liudd2016@126.com

Experimental

Powder and coating preparation

The starting raw materials were WC powder (99.8% purity, 2.9 μm, Luoyang Golden Egret Geotools Co., Ltd., China), WB powder (99.5% purity, 3.2 μm, Luoyang Golden Egret Geotools Co., Ltd., China), and Co powder (99.8% purity, 0.8 μm, Nanjing Hanrui Cobalt Co., Ltd., China). Based on the same process, WC-30WB-10Co composite powders and WC-12Co composite powders were fabricated. Initially, weighted powders were wet ball-milled in distilled water for 48 h with WC-8Co cemented carbide balls. The ball-to-powder mass ratio was set as 4:1 and polyethylene glycol (PEG) was employed as binder. Then, the obtained slurries were prepared into spherical particles by spray granulation and subsequently sintered at 1250 °C for 2 h under vacuum. After crushing and sieving, two kinds of spherical powders with particle size distribution of 15 μm-45 μm were obtained.

The low-carbon steel which had the dimensions of 100 mm × 100 mm × 5 mm was applied to be substrate materials. Initially, the substrates were initially blasted with Al_2O_3 (60-100 meshes) and subsequently cleaned with ethanol prior to spraying coating. The JP-8000 HVOF thermal spraying system was used for depositing the WC-30WB-10Co coating and WC-12Co coating. In addition, the same spraying parameters were used for two coatings. The kerosene flux, oxygen flux, carrier gas, powder feed rate and spraying distance were 0.39 L/min, 880 L/min, 10.8 L/min, 60 g/min, and 360 mm, separately.

Characterizations of feedstock powder and deposited coating

With the use of scanning electron microscopy, the microstructures of the powders, coating and wear tracks were analyzed (Evo18, Zeiss, Germany). Using X-ray diffraction (Dmax/2550VB+, Tokyo, Japan) with Cu-Kα radiation, the phase compositions of the powders and coatings were detected. Based on an image analysis software, the porosity of the coating was evaluated on the cross-section by a Metallurgical microscope (Imager. A2m, Zeiss, Germany). In addition, using a Vickers indenter (402 MVD, Wilson, USA) with the dwell time of 10 s and a load of 300 g, the microhardness of the coatings was identified on the polished cross-section. Ten indentations were performed for each sample.

With a reciprocating sliding tribometer, the sliding wear test of the coatings was carried out (UMT-2, Bruker, USA). In this study, a commercial WC-8Co ball with a diameter of 5 mm was employed as the counterpart. Prior to the testing, the coatings were ground and polished to obtain an average surface roughness in the range of 60-80 nm. The sliding wear tests were performed at the load of 10 N, the oscillating frequency of 4 Hz and the total sliding distance of 1500 m. With the temperature of 30±0.5 °C and the relative humidity of 50±2%, the sliding wear tests were performed. Based on of a 3D optical microscope (ContourGT-K, Bruker, USA), the wear volume of the coating was measured. In addition, according to the wear volume (mm^3) over the applied load (N) and the total sliding distance (m), we calculated the wear rate. By the average of three calculated values, we acquired the wear rate of the coating.

Results and Discussion

Microstructure and phase constitution

Fig. 1 illustrates SEM micrographs of the prepared feedstock particles. As shown in the figure, the two powders presented a highly spherical shape and smooth surface, which facilitated the powder feeding during spraying process.

Fig. 2 presents XRD patterns of the WC-30WB-10Co powders and WC-12Co powders. Obviously, it could be found in Fig. 2a that the CoWB phase and a tiny amount of CoW_2B_2 phase were detected besides WC, and the WB phase and Co phase were not detected. The new phase CoWB and CoW_2B_2 were formed using the reaction between WB and Co in the sintering process of initial powders, leading to the disappearance of WB phase and Co phase [14]. By contrast, compared with

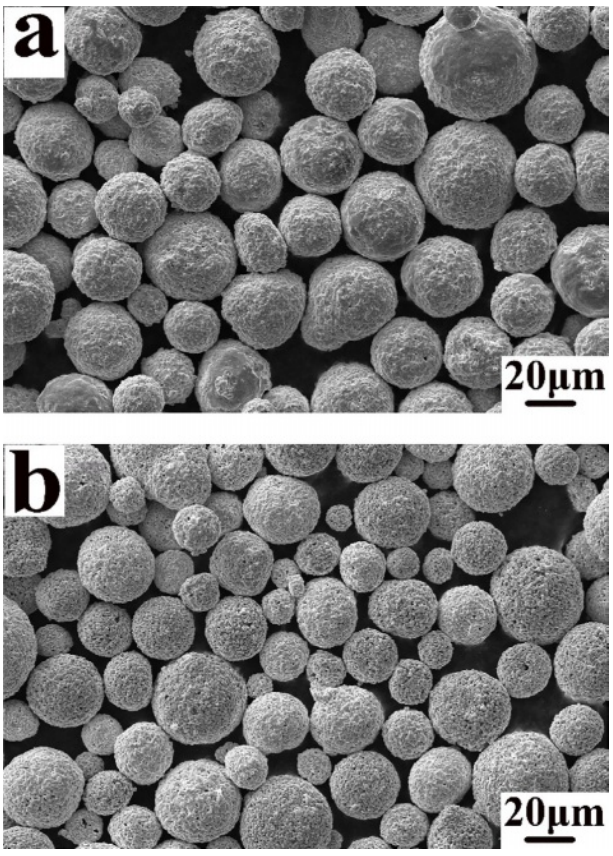

Fig. 1. SEM micrographs of (a) WC-30WB-10Co powders and (b) WC-12Co powders.

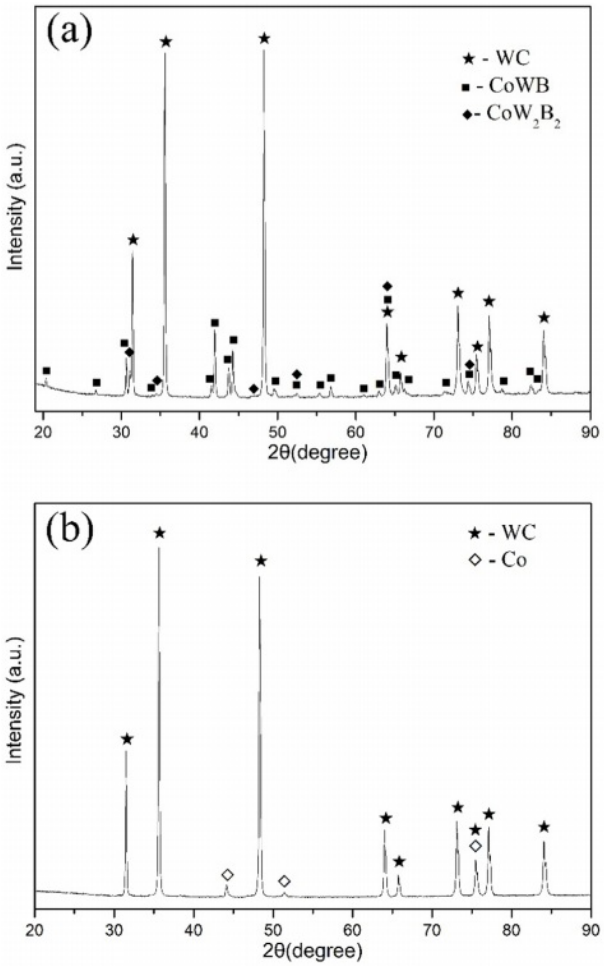

Fig. 2. X-ray diffraction patterns of (a) WC-30WB-10Co powders and (b) WC-12Co powders.

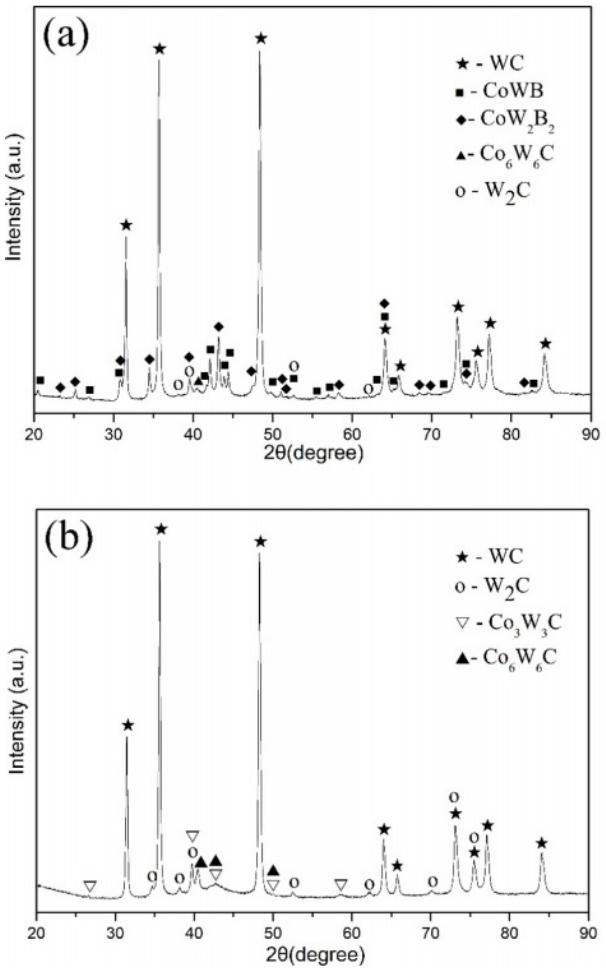

Fig. 3. X-ray diffraction patterns of (a) WC-30WB-10Co coating and (b) WC-12Co coating.

the initial powders, no new phases were formed in the WC-12Co powders.

XRD patterns of the both coatings are shown in Fig. 3. As shown, a small amount of W_2C, Co_3W_3C and Co_6W_6C could be detected in both coatings besides the phases mentioned above in Fig. 2. The formation of the new phases was caused by the oxidation and decomposition of WC in HVOF thermal spraying process [15-17]. It was worth noting in Fig. 3(b) that the Co diffraction peaks were not detected in relative to the powders. The disappearance of the Co phase was caused by the extremely high cooling rate of the molten particles, which led to the amorphization of Co phase during the solidification process. Some similar results were proposed for WC-Co coating [18-20].

Based on Fig. 4, both of the coatings exhibited very dense microstructure with few microscopic defects. The porosity measurement showed that the porosities of WC-30WB-10Co coatings and WC-12Co coatings were 0.56 vol.% and 0.73 vol.%, separately. The WC particles showed sub-angular and blocky shape in both the coatings. The CoWB phase was distributed in WC phase homogeneously in the WC-30WB-10Co coatings. In addition, the WC phase was surrounded by the Co metallic phase in the WC-12Co coatings.

Microhardness of coatings

The microhardness can profoundly affect the wear resistance of the coatings. On this basis, the microhardness of both coatings was obtained from ten indentations for each sample. According to the results presented in Fig. 8, the microhardness of WC-30WB-10Co coating was 1639HV0.3, indicating higher value in relative to the traditional WC-12Co coating with 1222HV0.3. The following factors were significantly associated with the higher hardness of WC-30WB-10Co coating. The microhardness of the coating depended on the microhardness and relative content of the constituent phases. The new phase CoWB was formed using the reaction between WB and Co, which led to the consumption of Co phase. The newly formed CoWB phase had higher hardness than the WC phase [14, 21]. The WC-30WB-10Co coatings contained around 60 wt% the WC phase, 40 wt% the CoWB phase with high hardness and very little Co metal phase with low hardness. In contrast, the WC-12Co coatings contained around 88 wt% the WC phase and 12 wt% the Co metal phase. In addition, the lower porosities, and the higher

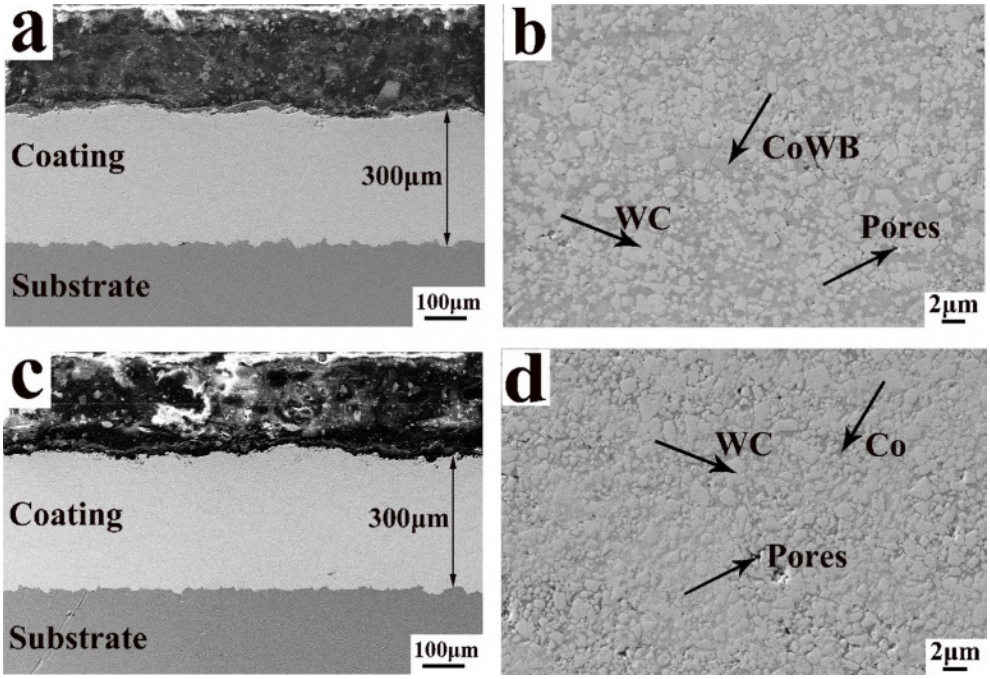

Fig. 4. Cross-sectional SEM micrographs of (a), (b) WC-30WB-10Co coating and (c), (d) WC-12Co coating: (a) and (c) ×100; (b) and (d) ×2000.

microhardness [22-24]. The WC-30WB-10Co coatings presented lower porosities compared with those of the WC-12Co coatings.

Wear performance of coatings

The increasing hardness of materials does not always mean the elevated wear resistance. On this basis, the sliding wear test of both coatings was carried out in our experiments. Fig. 5 illustrates the friction coefficient curves of the two coatings versus sliding distance. It was discovered that the friction coefficient curves of the two coatings were quite similar. Under the condition that the initial oxide films on the surface of the coatings were destroyed by sliding, the adhesion between the contacting surfaces was heavier. In the meanwhile, the two friction coefficient curves first went up. After that, the new oxide films were formed on the fresh surface due to friction heat, and then the two curves went down slightly. When the dynamic equilibrium between the wear and formation of oxide film was achieved, the two curves remained stable [25]. The average friction coefficients of both coatings were 0.51 and 0.45, respectively. Obviously, in relative to the WC-12Co coatings, the WC-30WB-10Co coatings exhibited the lower friction coefficient.

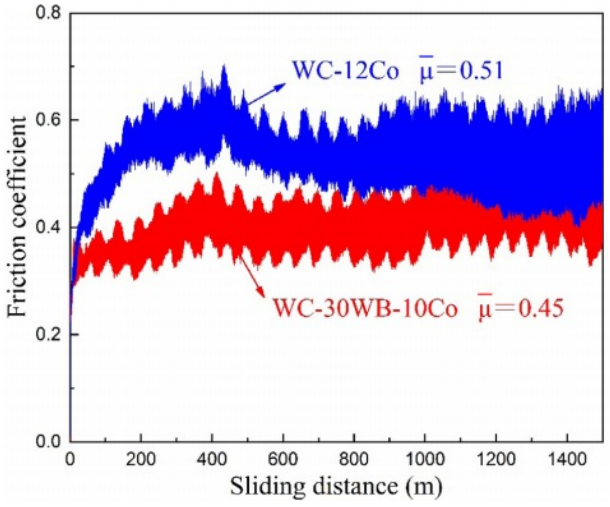

Fig. 5. Friction coefficients of WC-30WB-10Co coating and WC-12Co coating. The average friction coefficients were obtained from the data of the steady wearing stage.

Fig. 6 displays the SEM micrographs of wear tracks of the two coatings. As shown, the wear tracks of WC-12Co coatings were extremely rough and a large number of spalling pits and cracks existed on the surface. Comparing to the WC-12Co coatings, the amount of spalling pits in the WC-30WB-10Co coatings was obviously reduced, and had a relatively smooth surface. This indicated that the WC-30WB-10Co coatings underwent much less plastic deformation, which was in consistent with the lower friction coefficient of the WC-30WB-10Co coatings. Fig. 7 presents the wear scar profiles of the two coatings. Obviously, it could be seen that the cross-sectional depth of the WC-30WB-10Co coating was smaller than that of the traditional WC-12Co coating, suggesting that the WC-30WB-10Co coating did not undergo severe wear in dry friction.

The wear rates of both coatings are displayed in Fig. 8. Clearly, the wear rates of the WC-30WB-10Co

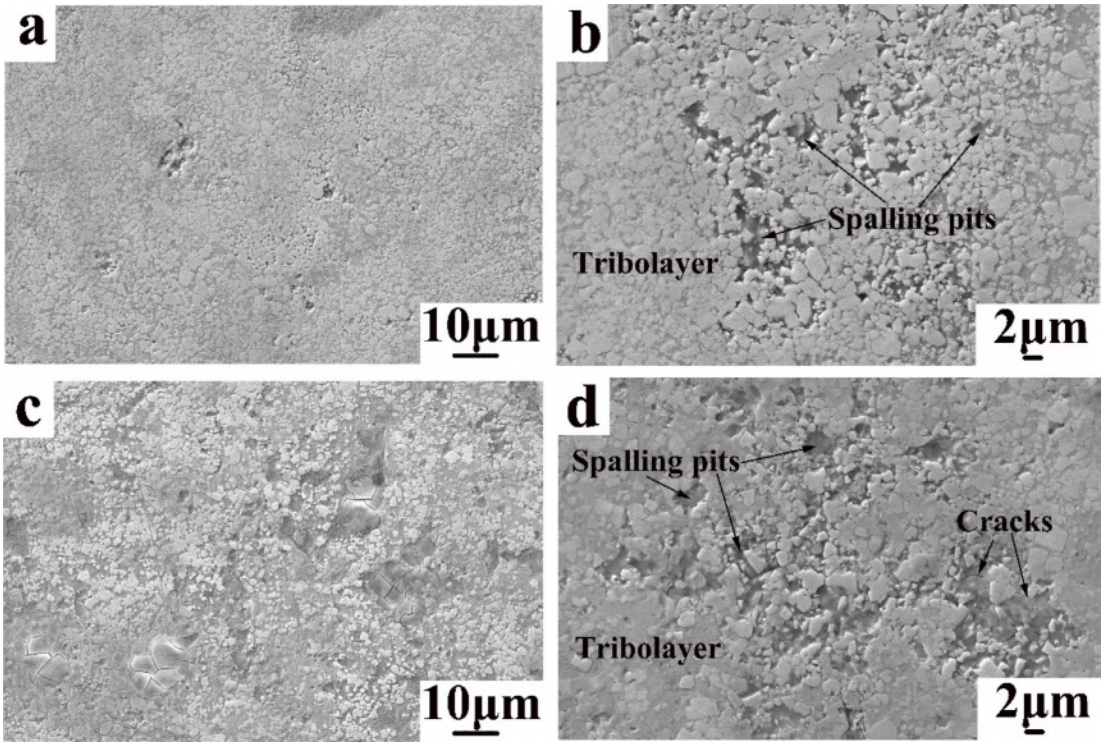

Fig. 6. SEM micrographs of wear tracks of (a), (b) WC-30WB-10Co coating and (c), (d) WC-12Co coating: (a) and (c) ×1000; (b) and (d) ×2000.

coatings and WC-12Co coatings were 4.09×10^{-8} mm^3/Nm and 8.29×10^{-8} mm^3/Nm respectively. The wear rates of the WC-30WB-10Co coating were only 49.3% of that of WC-12Co coatings. In relative to the WC-12Co coating, the WC-30WB-10Co coating showed excellent wear resistance. There are many factors which can affect the wear resistance of carbide-based coatings sprayed by HVOF [26]. In this study, the two feedstock particles and coatings were fabricated by the same process. Therefore, microstructure and phase composition were the leading reason for the different wear resistance of these two coatings. The surface of the coating and the WC-8Co ball was smooth before sliding wear test. During the early wear process of both coatings, some hard particles were cut out firstly, resulting in formation of spalling pits on the surface of the coatings (Fig. 6). Then, these pulled-out hard particles further participated in the wear process as abrasive particles leading to aggravating wear. Abrasive wear was the leading wear mechanism of the coatings. Under abrasive wear conditions, the hardness profoundly impacts the wear resistance of the coatings. Based on Fig. 8, owing to the formation of the superhard CoWB phase as well as the consumption of the ductile

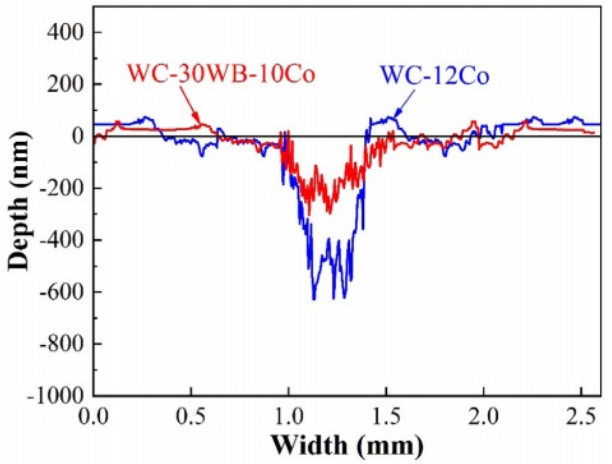

Fig. 7. Wear scar profiles of WC-30WB-10Co coating and WC-12Co coating.

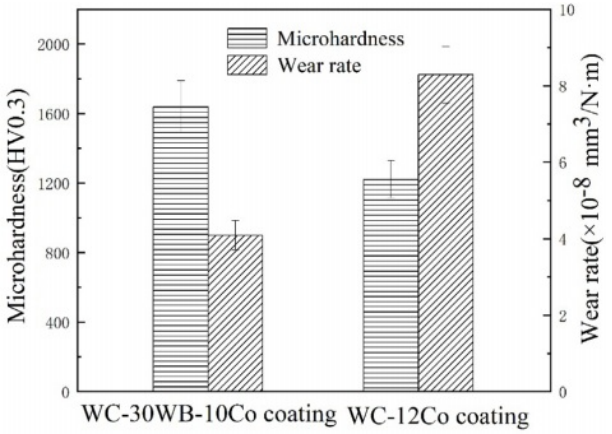

Fig. 8. Microhardness and wear rate of WC-30WB-10Co coating and WC-12Co coating.

Co binder, the WC-30WB-10Co coating possessed higher microhardness than the traditional WC-12Co coating. The high microhardness of the WC-30WB-10Co coating could effectively reduce the impressed depth of the WC-8Co counterpart, and protected the worn surface from being plowed, which weakened the degree of abrasive wear. Meanwhile, the wettability between CoWB and WC was better than that between WC and Co [27]. This could effectively restrain the hard particles from being pulled out of the coatings. Thus, the WC-30WB-10Co coating showed better wear resistance in relative to the WC-12Co coating in the early friction process. Based on the repeated sliding process, oxidation gradually occurred on the surface of the coating owing to the friction-induced temperature rise. The Co binder phase in the WC-12Co coatings was preferentially oxidized to form CoO due to the poor oxidation resistance. The formation of CoO further promoted the oxidation of WC phase to form $CoWO_4$. Subsequently, the oxidized particles were easily pulled out of coating due to the lack of the binder constraint. These pulled out particles continued to act as abrasive particles to exacerbate the wear of WC-12Co coatings in the subsequent wear cycles. In addition, owning to the oxidation-induced expansion stress, it could be seen from Fig. 6c and d that some cracks were formed [28]. When these cracks joined together, flaky exfoliation happened from the surface of the WC-12Co coating. This was the primary cause of severe wear of the WC-12Co coating. In contrast, the Co phase did not exist in the WC-30WB-10Co coating owing to the formation of the ternary CoWB and CoW_2B_2 compound (as shown in Fig. 3). The oxidation of WC phase was significantly inhibited due to the absence of cobalt oxides (such as CoO). The CoWB and CoW_2B_2 phase had higher oxidation resistance than the Co binder phase [29], which could simultaneously protect the WC phase from oxidation. This could inhibit the pulling out of hard particles and the formation of cracks, and thus very few cracks were observed in the WC-30WB-10Co coating during the wear process. All this could significantly decrease the wear rate of the WC-30WB-10Co coating. Thus, the WC-30WB-10Co coating showed excellent wear resistance when compared with the WC-12Co coating. Abrasive wear and oxidative wear were the wear mechanisms of both coatings. The developed WC-30WB-10Co coating is expected to be well applied under aggressive wear and corrosion conditions due to its excellent wear resistance and low metal phase content.

Conclusions

To conclude, in this study, the morphologies, phase composition, hardness, as well as sliding wear performance of the WC-30WB-10Co coatings were explored. We made the main conclusions.

(1) The CoWB phase as well as a very small quantity of CoW_2B_2 phase were identified. We found that few new phases existed in the WC-12Co powders. In HVOF spraying of the powder, the oxidation and decarburization happened according to the existence of the diffraction peaks of W2C, Co3W3C and Co6W6C in the two coatings.

(2) It was found that the microhardness of the WC-30WB-10Co coating was1639HV0.3, indicating higher value in relative to the traditional WC-12Co coating with 1222HV0.3. In addition, the formation of the ternary CoWB compound as well as the consumption of the ductile Co binder could lead to the high microhardness of the WC-30WB-10Co coating.

(3) In relative to the traditional WC-12Co coating, the wear resistance of the WC-30WB-10Co coating was greatly enhanced. The wear rates of the WC-30WB-10Co coating were only 49.3% of that of WC-12Co coatings.

Acknowledgements

The current work was supported by the Scientific Research Fund of Hunan Provincial Education Department (23A0614) and the Hunan Provincial Enterprise Science and Technology Correspondent Fund Project (2021GK5028).

References

1. X. Luo, G.M. Smith, Y. Wang, E. Gildersleeve, S. Sampath, and C. Li, Ceram. Int. 45 (2019) 4718-4728.
2. X. Wang, X. Ping, X. Zeng, R. Wang, Q. Zhao, S. Ying, and T. Hu, Surf. Coat. Technol. 441 (2022) 128555.
3. X. Lu, Z. Lin, P. Pan, Y. Chen, L. Zuo, and C. Li, J. Ceram. Process. Res. 22 (2021) 649-654.
4. M.Y. Maximov, A.S. Verevkin, A.A. Orlova, P.A. Novikov, A.O. Silin, O.V. Panchenko, and A.A. Popovich, J. Ceram. Process. Res. 18 (2017) 103-107.
5. K. Derelizade, F. Venturi, R.G. Wellman, A. Kholobysov, and T. Hussain, Wear 482-483 (2021) 203974.
6. Z. Geng, S. Li, D.L. Duan, and Y. Liu, Wear 330-331 (2015) 348-353.
7. J. Liu, T. Chen, C. Yuan, and X. Bai, J. Therm. Spray. Techn. 29 (2020) 798-810.
8. H. Wang, Q. Qiu, M. Gee, C. Hou, X. Liu, and X. Song, Mater. Des. 191 (2020) 108586.
9. D. Mohanty, S. Kar, S. Paul, and P.P. Bandyopadhyay, Mater. Des. 156 (2018) 340-350.
10. P. Mi and F. Ye, Int. J. Refract. Met. H 76 (2018) 185-191.
11. J.H. Lee and H.K. Park, J. Ceram. Process. Res. 22 (2021) 655-664.
12. J. Chrzanowska-Giżyńska, P. Denis, M. Giżyński, Ł. Kurpaska, I. Mihailescu, C. Ristoscu, Z. Szymański, and T. Mościcki, Appl. Surf. Sci. 478 (2019) 505-513.
13. M. Usta, I. Ozbek, M. Ipek, C. Bindal, and A.H. Ucisik, Surf. Coat. Technol. 194 (2005) 330-334.
14. Z.T. Zahariev and M.I. Marinov, J. Alloys. Compd. 201 (1993) 1-3.
15. D. Lou, J. Hellman, and D. Luhulima, Mater. Sci. Eng. A 340 (2003) 155-162.

16. Q. Wang, Z. Chen, L. Li, and G. Yang, Surf. Coat. Technol. 206 (2012) 2233-2241.
17. T.K. Mishra, A. Kumar, S.K. Sinha, and S. Sharma, Mater. Today: Proceedings 5 (2018) 19539-19546.
18. S. Sampath and H. Herman, J. Therm. Spray. Techn. 5[4] (1996) 445-456.
19. D.A. Stewart, P.H. Shipway, and D.G. McCartney, Acta Mater. 48[7] (2000) 1593-1604.
20. Q. Wang, J. Xiang, G. Chen, Y. Cheng, X. Zhao, and S. Zhang, J. Mater. Process. Tech. 213 (2013) 1653-1660.
21. A. Saez, F. Arenas, and E. Vidal, Int. J. Refract. Met. H 21 (2003) 13-18.
22. I. Baumann, L. Hagen, W. Tillmann, P. Hollingsworth, D. Stangier, G. Schmidtmann, M. Tolan, M. Paulus, and C. Sternemann, Surf. Coat. Technol. 405 (2021) 126716.
23. J.H. Lee, J.C. Park, B.S. Park, and H.K. Park, J. Ceram. Process. Res. 24 (2023) 216-221.
24. D. Ghahremani, I. Mobasherpour, M. Razavi, H. Eslami Shahed, and H. Rajaei, J. Ceram. Process. Res. 17 (2016) 1143-1147.
25. J.A.R. Wesmann and N. Espallargas, Tribol. Int. 101 (2016) 301-313.
26. W. Zhou, K. Zhou, Y. Li, C. Deng, and K. Zeng, Appl. Surf. Sci. 416 (2017) 33-44.
27. H. Wang, X. Yan, X. Liu, H. Lu, C. Hou, X. Song, and Z. Nie, J. Eur. Ceram. Soc. 38 (2018) 4874-4881.
28. S.N. Basu and V.K. Sarin, Mater. Sci. Eng. A 209 (1996) 206-212.
29. X. Liu, Z. Liang, H. Wang, Z. Zhao, C. Liu, H. Lu, and X. Song, Met. Hard Mater. 105 (2022) 105827.